Brazilian Journal of Physics
ISSN: 0103-9733
luizno.bjp@gmail.com
Sociedade Brasileira de Física
Brasil

Kesavan, K.; Mathew, Chithra M.; Rajendran, S.; Subbu, C.; Ulaganathan, M.
Solid Polymer Blend Electrolyte Based on Poly(ethylene oxide) and Poly(vinyl pyrrolidone) for Lithium Secondary Batteries
Brazilian Journal of Physics, vol. 45, núm. 1, 2015, pp. 19-27
Sociedade Brasileira de Física
Sâo Paulo, Brasil

Available in: http://www.redalyc.org/articulo.oa?id=46433753003

How to cite
Complete issue
More information about this article
Journal's homepage in redalyc.org

Scientific Information System
Network of Scientific Journals from Latin America, the Caribbean, Spain and Portugal
Non-profit academic project, developed under the open access initiative

Braz J Phys (2015) 45:19–27
DOI 10.1007/s13538-014-0279-6

CONDENSED MATTER

Solid Polymer Blend Electrolyte Based on Poly(ethylene oxide) and Poly(vinyl pyrrolidone) for Lithium Secondary Batteries

K. Kesavan · Chithra M. Mathew · S. Rajendran · C. Subbu · M. Ulaganathan

Received: 2 July 2014 Published online: 30 October 2014
© Sociedade Brasileira de Física 2014

Abstract Solid polymer electrolytes have attracted considerable attention due to their wide variety of electrochemical device applications. In the present study, the fixed concentration of the salt lithium perchlorate ($LiClO_4$) and various concentrations of poly(ethylene oxide)/poly(vinyl pyrrolidone) (PEO/PVP)-based electrolytes were prepared by solvent casting technique. The structural analysis of the present system shows that the amorphous character of the samples is responsible for the process of ion transport. Fourier transform infrared spectroscopy (FTIR) has been used to characterize the structure of polymer and confirm the complexation between the polymers and salt. The maximum ionic conductivity value is found to be 0.2307×10^{-5} S cm^{-1} for PEO (90 wt%)/PVP (10 wt%)/$LiClO_4$ (8 wt%) (A1) complex at 303 K (30 °C).

Keywords Polymer electrolyte · Ionic conductivity · Luminescence · Band gap · Thermal stability

1 Introduction

Thanks to today's advanced science and technological development, many types of renewable or green energy sources such as wind, water, and solar energy have been developed. However, due to the rapid increment of mobile device usage, from a light mp3 player, mobile devices, to the heavy duty electric vehicle power back, the usage of those power sources is very frequent and repeated.

Hence, the development of secondary rechargeable battery is considerably more important as compared to primary batteries. It is desirable to manufacture a small-sized, high-capacity, and lightweight battery which is environmental friendly and renewable. In this paper, the attention has been focused on the polymer electrolyte due to its high ionic conductivity as well as good mechanical properties [1, 2]. The presence of solid polymer electrolytes eliminates the leakage and flammable as compared to liquid electrolytes.

However, solid polymer electrolytes (SPEs) for lithium ion secondary batteries mainly involve lithium salt complexes solvated by some polymer. Depending on the characteristics of the polymer host, SPEs exhibit stronger safety features and better compatibility with lithium metal anodes and increase availability for flexible battery shape designs than liquid electrolytes.

Ionic conductivity in poly(ethylene oxide) (PEO) alkali metal salt complexes was first reported by Wright [3] in 1972. Armand [4] presented the idea of constructing solid lithium batteries. Poor ambient temperature ionic conductivity (10^{-8}–10^{-7} S cm^{-1}) and low cation transference number (<0.3) are the two major drawbacks for PEO-based SPEs. An important progress was made by Croce [5, 6] who developed nanomaterial-enriched SPEs in the 1990s.

In recent years, PEO has been extensively studied as an electrolyte and separator materials for its outstanding film-forming and good lithium ion stability. The polymeric chain of PEO is capable of wrapping around the lithium ion, creating coordination bonds [7, 8]. PEO is a semicrystalline polymer, possessing both amorphous and crystalline phases at room temperature. It can solvate a wide variety of salts even at very high salt concentrations. The suppression of crystallinity of

K. Kesavan · C. M. Mathew · S. Rajendran (✉) · C. Subbu
School of Physics, Alagappa University, Karaikudi, Tamilnadu 630003, India
e-mail: sraj54@yahoo.com

M. Ulaganathan
Energy Research Institute @ NTU, Nanyang Technological University, Singapore 637 553, Republic of Singapore

polymer chains improves the polymer chain mobility which in turn leads to better ionic conduction.

Polymer blending is one of the effective methods to reduce crystalline content and enhance the amorphous content. Polyblends often exhibit properties that are superior to the individual component polymers [9].

Poly(vinyl pyrrolidone) (PVP) was selected as the second polymer component for preparing a polymer blend with a PEO, because of its unique characteristics. PVP is a special one among the conjugated polymers because of its high amorphous nature which can permit faster ionic mobility. The presence of the carbonyl group (C=O) in PVP leads to form a variety of complexes with various inorganic salts and exhibits high T_g with good environmental, thermal, and mechanical stability [10]. Furthermore, PVP is highly soluble in polar solvents such as alcohol.

In our previous work, we have studied the effect of different lithium salts having various cation size in PEO/PVP blend electrolytes, in which the maximum conductivity was obtained for the electrolyte sample with $LiN[CF_3SO_2]_2$ (LiTFSI) salt [11]. The reported reason for the conductivity variation is the difference in lattice energies of the lithium salts. The changes in optical band gap and photoluminescence intensity of the samples confirm the same result. So, in order to find the optimal blend combination between PEO and PVP, we have attempted to prepare polymer electrolytes with 90:10, 80:20, 70:30, and 60:40 ratios of PEO/PVP and 8 wt% of $LiClO_4$. Even though LiTFSI exhibits so many merits, the application of lithium imide in lithium ion cells never materialized because it caused severe Al corrosion in electrolytes based on it. Since the role of Al as a cathode substrate in the lithium-based battery industry is hard to replace, due to its light weight, resistance to oxidation at high potential, excellent processability, and low cost, the imide ion greatly restricts the possible application of LiTFSI [12]. Hence, relatively being less hygroscopic, $LiClO_4$ is used in the present study. The choice of choosing $LiClO_4$ is due to its smaller ionic radius, smaller dissociation energy, and the high solubility in most of the inorganic solvents [13].

2 Materials and Method

PEO (~M_w, 8,000), PVP (~M_w, 360,000), and $LiClO_4$ were purchased from Aldrich Chemicals Limited, USA. Polymer electrolytes of various blend ratios were prepared by solvent casting technique with methanol as a solvent. The polymer PEO was dissolved at 50 °C in the solvent methanol, and PVP was dissolved at room temperature, respectively. The dissolved polymers were mixed together. After that, the salt $LiClO_4$ was added into the polymer complex. The complex was stirred well for 24 h with the help of a magnetic stirrer and degassed to remove air bubbles. Finally, the solution was cast on a Petri dish, and the solvent was allowed to evaporate slowly at room temperature for 48 h. This procedure yielded free standing and flexible films. Flexible thin films with a thickness of about 0.1–0.5 mm were obtained. Blends of PEO/PVP were prepared in different weight ratios (90:10, 80:20, 70:30, and 60:40) with a constant salt concentration with a view to optimize the blend ratio on the basis of ionic conductivity and thermal stability of the films.

3 Measurements

The nature of the materials and the dissolution of the salt could be determined by an X-ray diffractometer (XRD). Laboratory X-ray diffraction of the nature of the materials and the dissolution of the salt was acquired at room temperature with X'pert PRO PANalytical diffractometer using Cu Kα radiation as source and operated at 40 kV. The sample was scanned in the 2θ ranging from 10° to 80° for 2 s in the step scan mode. The Fourier transform infrared spectroscopy (FTIR) spectra of the polymer electrolytes were recorded at room temperature in the range of 400–4,000 cm^{-1} using SPECTRA RXI, PerkinElmer spectrophotometer. Conductivity studies were carried out with the help of stainless steel blocking electrodes using a computer-controlled micro auto lab type III potentiostat/galvanostat in the frequency range of 100 Hz–300 KHz over the temperature range of 303–353 K. A PYRIS DIAMOND under air atmosphere with the scan rate of 10 °C min^{-1} was used for the thermogravimetric analysis of the samples. Ultraviolet–visible (UV–Vis) absorption spectra were measured in the wavelength region 190 to 900 nm by Shimadzu UV-1601. The surface morphology of the sample was obtained from atomic force microscopy (AFM) using AFM (A100SGS). The photoluminescence studies were performed by Cary Eclipse fluorescence spectrophotometer.

4 Results and Discussion

4.1 X-ray Diffraction Studies

XRD studies were performed on pure PEO, PVP, $LiClO_4$, and PEO/PVP/$LiClO_4$-based complexes in order to investigate the structure of the polymer electrolytes. Figure 1a of $LiClO_4$ shows high intense peaks at angles 2θ=20.9°, 22.92°, 26.56°, 32.75°, and 35.4° which reveal the crystalline nature of the ionic salt. Two broad peaks around 19.2° and 23.5° for PEO in Fig. 1b confirm the semicrystalline nature. A halo peak around 22.7° which is attributed to the amorphous nature of pure PVP is shown in Fig. 1c. It is seen that crystallinity of the blended complex decreases with the addition of PVP. However, on the addition of the lithium salt to the polymer blend, the intensity of these peaks decreases gradually and

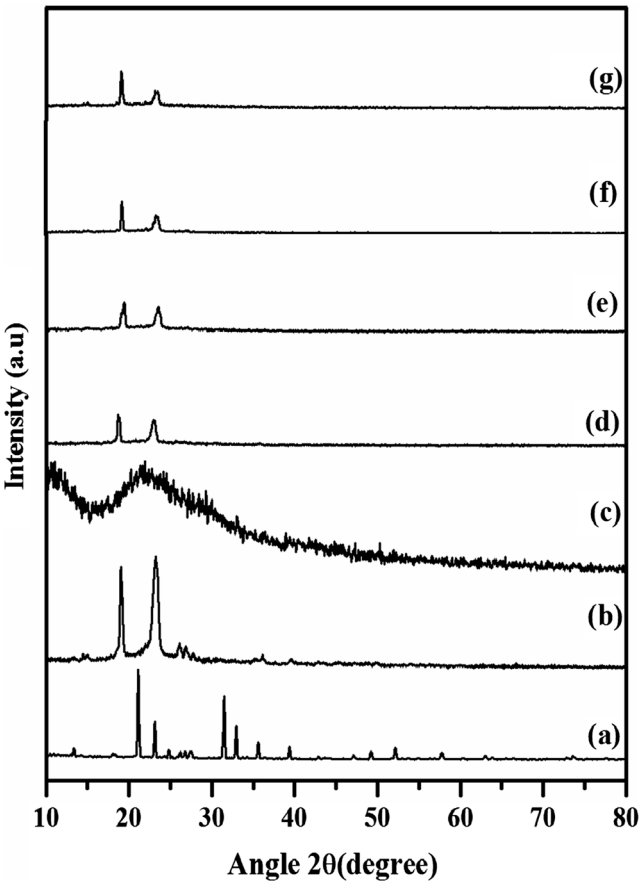

Fig. 1 XRD patterns of (*a*) pure $LiClO_4$, (*b*) pure PEO, (*c*) pure PVP, (*d*) A1, (*e*) A2, (*f*)A3, and (*g*) A4

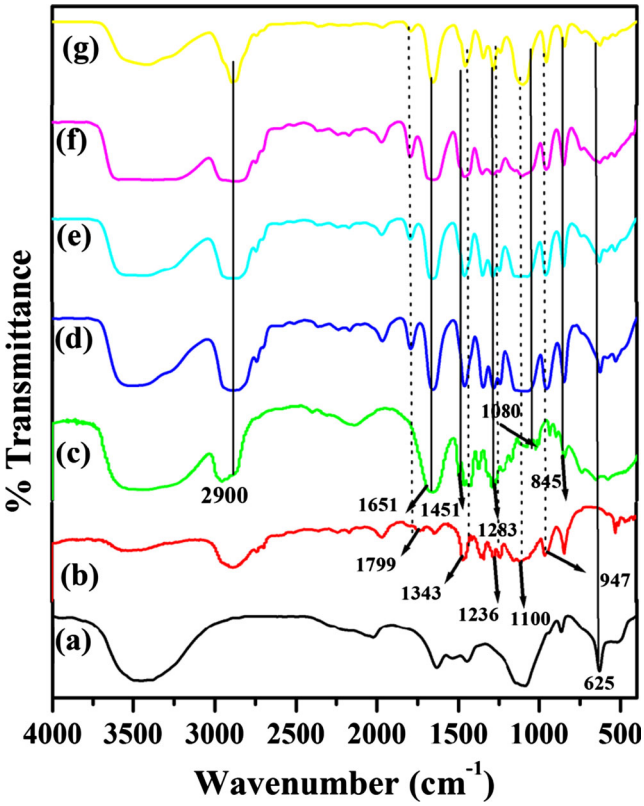

Fig. 2 FTIR spectra of (*a*) pure $LiClO_4$, (*b*) pure PEO, (*c*) pure PVP (*d*) A1, (*e*) A2, (*f*) A3, and (*g*) A4

becomes relatively broader, suggesting a decrease in the degree of crystallinity of the complex. Hence, the absence of peaks pertaining to $LiClO_4$ salt in the complexes indicates the complete dissolution of the salt in the polymer matrix. This shows that $LiClO_4$ does not form any separate phase in the complex system.

4.2 FTIR Analysis

Infrared analysis is a powerful tool to identify the nature of bonding and different functional groups in a sample by monitoring the vibrational energy levels of the molecules, which are essentially the fingerprint of different molecules [14, 15].

Figure 2 shows the FTIR transmittance spectra of the present samples recorded at room temperature in the region 4,000–400 cm^{-1}. The spectra exhibit band characteristic of stretching and bending vibrations of the films. FTIR absorption band positions and the assignment of all the prepared samples are listed in Table 1.

From the spectra, for pure PEO, a very small intense band at 1,799 cm^{-1} corresponds to the ether oxygen group [16] which is shifted to 1,792, 1,790, 1,790, and 1,791 cm^{-1} in all the complexes, respectively. The band at 1,343 cm^{-1} is due to CH_2 bending of PEO [17]. The strong interaction in PEO is the asymmetric CH_2 twisting at 1,282 cm^{-1} which is shifted to 1,282, 1,284,1,282, and 1,284 cm^{-1} in all the complexes, respectively. The relatively small band at around 1,236 cm^{-1} is assigned to CH_2 symmetric twisting of PEO [16]. The characteristic vibration band at 1,100 cm^{-1} is assigned to C-O-C (symmetric and asymmetric) stretching of PEO [16] which is shifted to 1,080, 1,099, 1,112, and 1,100 cm^{-1}, respectively, in all the complexes. Apart from this, the mode responsible for the band at 845 cm^{-1} is primarily due to the CH_2-rocking motion with a little contribution from C–O stretching motion of PEO, while band at 947 cm^{-1} originates primarily in the C–O stretching motion with some CH_2-rocking motion [18].

On the other hand, for pure PVP, a vibrational band observed at 2,900 cm^{-1} may also be attributed to aliphatic C–H stretching of PVP [19] which is shifted to 2,885, 2,897, 2,868, and 2,892 cm^{-1} in all the A1, A2, A3, and A4 complexes, respectively. The bands around 1,651 and 1,451 cm^{-1} are attributed to C=O stretching and CH_2 wagging of pure PVP which are shifted to 1,654, 1,654, 1,654, and 1,654 cm^{-1} and 1,461, 1,459, 1,456, and 1,456 cm^{-1} of the all complexes, respectively.

A band at 1,283 cm^{-1} which corresponds to CH_2-wagging motion of pure PVP is shifted to 1,282, 1,284, 1,282, and 1,284 cm^{-1} in A1, A2, A3, and A4, respectively [20]. The

Table 1 FTIR spectral data of the pure and prepared complexes

Band assignments	Wave number (cm^{-1})					
	PEO	PVP	A1	A2	A3	A4
Aliphatic C–H stretching	–	2,900	2,885	2,897	2,868	2,892
Ether oxygen group	1,799	–	1,792	1,790	1,790	1,791
C=O stretching	–	1,651	1,654	1,654	1,654	1,654
CH_2 wagging	–	1,451	1,461	1,459	1,456	1,456
CH_2 bending	1,343	–	1,347	1,347	1,349	1,346
CH_2 asymmetrical stretching in PEO and CH_2 wagging in PVP	1,282	1,283	1,282	1,284	1,282	1,284
CH_2 symmetrical twisting	1,236	–	1,243	1,243	1,243	1,242
C–O–C symmetrical and asymmetrical stretching in PEO and C–C stretching in PVP	1,100	1,080	1,099	1,112	1,098	1,100
C–O stretching motion with some CH_2-rocking motion	947	–	953	954	952	954
CH_2 rocking in PVP and with some C–O stretching in PEO	845	845	845	846	844	845
ClO_4^-	–	–	625	625	625	625

vibrational band at 1,080 cm^{-1} in pure PVP assigned to C–C bending is shifted to 1,099, 1,112, 1,098, and 1,100 cm^{-1} in all the complexes, respectively. The band at 845 cm^{-1} attributed to CH_2 rocking of pure PVP which is shifted to 845, 846, 844, and 845 cm^{-1} in the A1, A2, A3, and A4 complexes, respectively. The FTIR spectrum of the $LiClO_4$ salt is given in Fig. 2a. The band at 625 cm^{-1} corresponds to ClO_4^- anion. The broad band of medium intensity at >500 cm^{-1} is due to ClO_4^-, which has become infrared active [21] and the band at 625 cm^{-1} is present in all the prepared complexes.

In addition, some new peaks are present, and some of them disappeared in the blended electrolytes. Thus, the spectral analysis confirms the complexation of these two polymers and lithium salt.

4.3 Conductivity Analysis

4.3.1 Impedance Spectroscopic Analysis

Figure 3 shows the complex impedance spectra for the prepared electrolytes at room temperature. The disappearance of semicircular portion in the high-frequency region of the complex impedance plot indicates that the conduction is mainly due to ions and the inclined line due to the effect of the blocking electrodes [22]. At low frequency, the impedance should exhibit a straight line parallel with the imaginary axis, but the double layer at the blocking electrodes causes the inclined line. The arc's intercept on the real axis gives the value of the bulk resistance (R_b). The ionic conductivity of the solid polymer electrolyte is calculated using the equation $\sigma = l/R_b A$, where l is the thickness of the polymer electrolyte film and A is the surface area of the film.

The conductivity values obtained for all the blend polymer electrolyte films in the temperature range of 303–353 K (30–80 °C) are listed in Table 2. The maximum room temperature ionic conductivity value 0.2307×10^{-5} S cm^{-1} is obtained for the sample A1. From Table 2, it is observed that when PVP ratio increases from 10 to 40 wt% in the polymer complexes, the ionic conductivity decreases. This may be due to a decrease in ionic mobility and hindrance of the polymer segmental motion. An increase of PVP content imparts higher viscosity and makes the mixture a rubbery transport solid. An increase in viscosity could also be realized as a macroscopic interaction effect between the polymer and solution which affects the mobility. Similar observations have already been reported by Bajpai et al. [23] and Rajendran et al. [24].

4.3.2 Temperature-Dependent Ionic Conductivity

Figure 4 shows the temperature-dependent ionic conductivity of the polymer salt complexes. From the plot, it is evident that as the temperature increases, the values of conductivity are increased for all the samples. This is in agreement with free volume theory [25]. This theory is, at higher temperatures, thermal movement of polymer chain segments and the dissociations of salts would be improved, which increased ionic conductivity for the prepared samples. However, at low temperatures, the presence of lithium salt leads to salt–polymer or cation–dipole in the polymeric networks. As the free volume was decreased, polymer segmental motion and ionic mobility were hindered and then the ionic conductivity decreased. As the temperature increases, the polymer can expand easily and produce free volume. Thus, ion-solvated molecules or polymer segments can move to the free volume. So, according to the free volume theory of polymers, when the temperature is increased, the vibrational energy of a segment is sufficient to push against the hydrostatic pressure imposed by its neighbors and create a small amount of space surrounding its own volume in which vibrational motion occur. The nonlinear variation of the temperature dependence conductivity plot

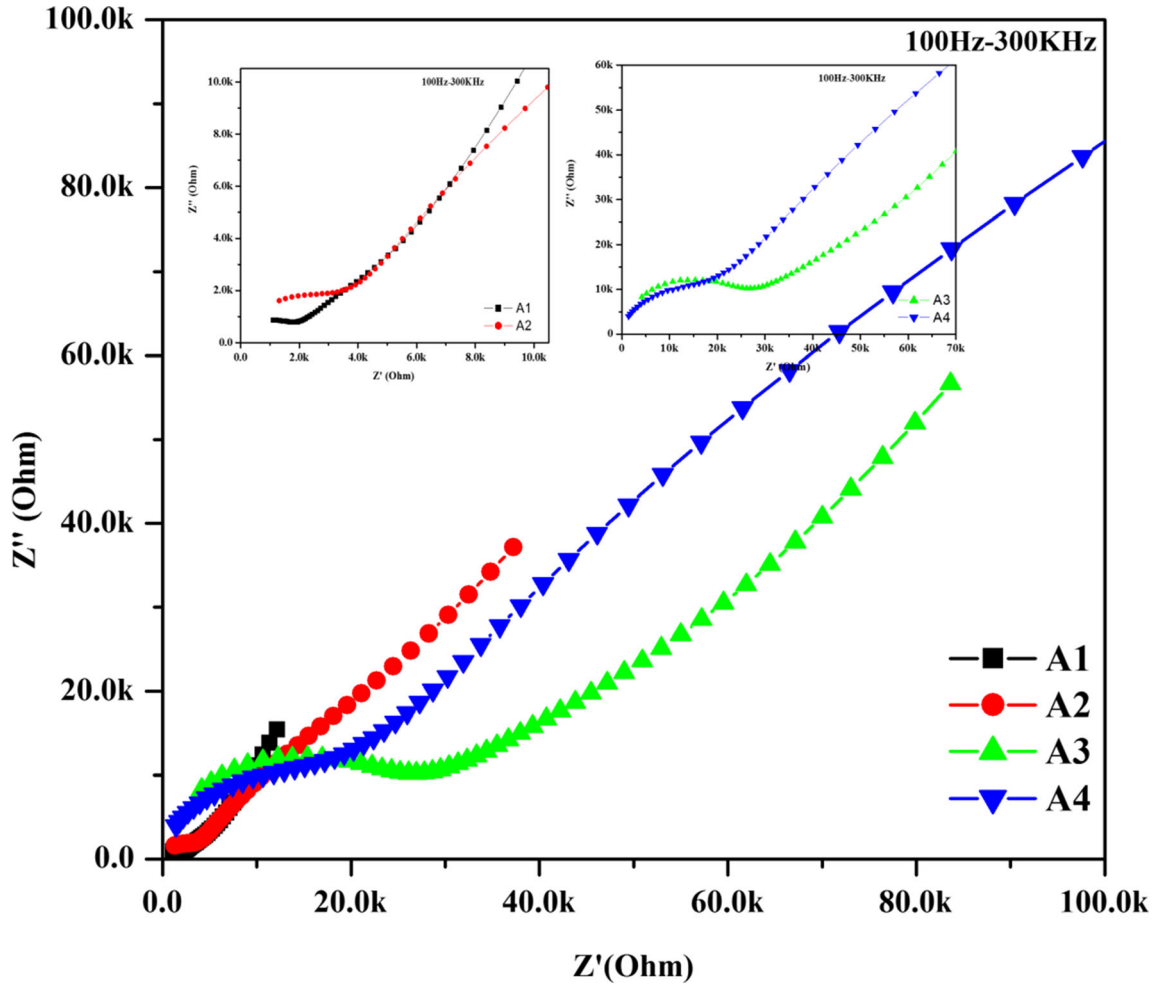

Fig. 3 Room temperature complex impedance plot of the prepared samples

suggests that the ion transport in polymer electrolytes depends on the polymer segmental motion. They cannot be described by the Arrhenius relationship but possibly by the Vogel-Tamman-Fulcher (VTF) expression based on the free volume concept [26].

4.4 TG/DTA Analysis

Thermal stability of the polymer electrolyte being an important parameter for guaranteeing acceptable performance during high-temperature operation has been studied using TGA.

Figure 5a–d shows thermogravimetric/differential thermal analysis (TG/DTA) thermograms of weight loss as a function of temperature for PEO/PVP/$LiClO_4$ at various concentrations with a heating rate of 10 °C/min in the temperature range from room temperature to 700 °C. TG/DTA results of all the prepared samples are shown in Table 3. It is clear that the initial weight loss for all the samples occurs at 76–82 °C due to the removal of moisture during sample loading process, and they

Table 2 Temperature-dependent ionic conductivity values of the prepared complex

Sample code	wt% compositions of [PEO/PVP] + $LiClO_4$	Ionic conductivity values (σ)×10^{-5} S cm^{-1} at different temperatures					
		303 K	313 K	323 K	333 K	343 K	353 K
A1	[90/10]+8	0.2307	0.3772	0.5353	1.2645	8.1513	10.2533
A2	[80/20]+8	0.1778	0.2539	0.3662	0.5548	2.1073	3.5313
A3	[70/30]+8	0.0628	0.0773	0.1893	0.3979	1.2425	2.5622
A4	[60/40]+8	0.0404	0.0614	0.1509	0.3450	0.7864	1.1763

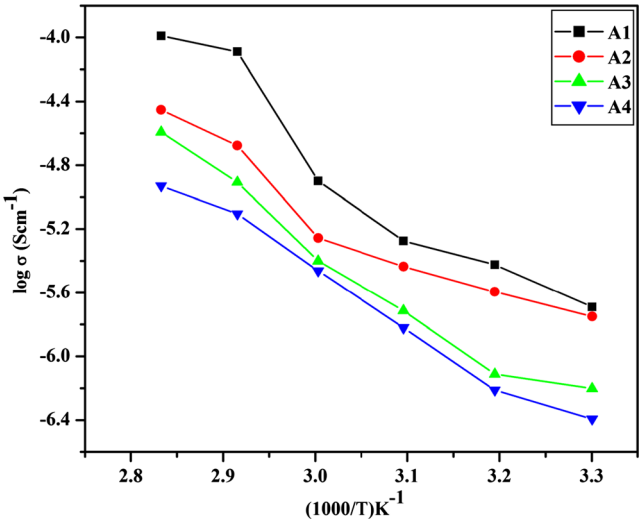

Fig. 4 Temperature-dependent ionic conductivity plot of the prepared samples

are stable up to 356 °C. The major weight losses are observed in the range of 324–356 °C for all the samples. This may be due to the structural decomposition of the polymer blends.

From the thermogram, it has been observed that the sample having a maximum ionic conductivity (A1) is thermally stable up to 324 °C. The sample starts to decompose at 340 °C; beyond which, there is a gradual weight loss of 14 % in the temperature range of 323–343 °C. However, the sample A2 is thermally stable up to 340 °C, which is higher compared to the other three samples. DTA curves of all the samples show exothermic peaks at 335–355 °C which are well correlated with the weight loss of all the samples observed in TG curve.

4.5 Optical Absorption (UV–Vis Analysis)

4.5.1 Absorption Vs. Wavelength

UV–visible spectra in the wavelength range of 190–400 nm of the polymer systems is shown in Fig. 6. In the UV region, the band around 195 nm has been observed for all the prepared samples. This absorption peak may be attributed to the $n \rightarrow \sigma^{+}$ transition which is very sensitive to hydrogen bonding. The absorption band around 227 nm may be assigned as $\pi \rightarrow \pi^{*}$, which comes from unsaturated bonds mainly C=O [27].

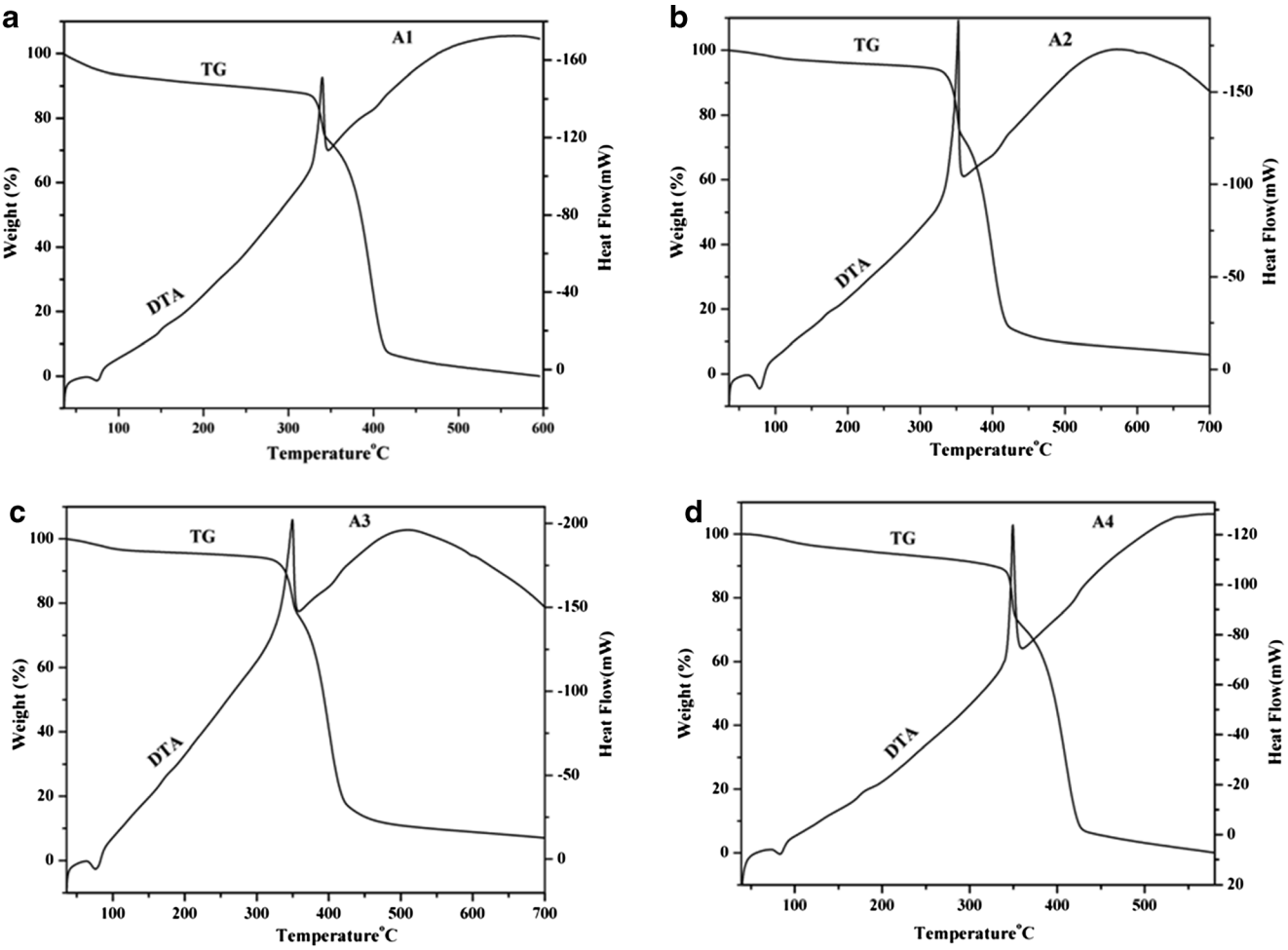

Fig. 5 TG/DTA analysis of the prepared complexes **a** A1, **b** A2, **c** A3, and **d** A4

Table 3 TG/DTA results of the prepared samples

Sample code	wt% compositions of [PEO/PVP] + $LiClO_4$	Decomposition temperature (°C)			Percent weight loss of the samples			Exothermic peaks (°C)		
		I	II	III	I	II	III	I	II	III
A1	[90/10]+8	76	340	418	6	22	95	75	339	–
A2	[80/20]+8	80	356	452	4	24	93	78	352	–
A3	[70/30]+8	82	356	421	5	22	92	77	349	–
A4	[60/40]+8	75	335	428	6	23	96	71	339	–

Figure 6 shows a shift in absorption edge toward the higher wavelength. These shifts in the absorption edge may be assigned to presence of Li-ions in the prepared samples. These bands reflect the variation of the energy band gap, which arises due to the variation in crystallinity within the polymer matrix [28].

4.5.2 Determination of Optical Band Gap (E_g)

The study of optical absorption gives information about the band structure of organic compounds. There are two types of band gaps: (i) direct band gap and (ii) indirect band gap. In the direct band gap, the top of the valence band and the bottom of the conduction band both lie at same zero crystal momentum. If the bottom of the conduction band does not correspond to zero crystal momentum, then it is called an indirect band gap semiconductor. In indirect band gap materials, transition from valance to conduction band should always be associated with a phonon of the light magnitude of crystal momentum.

Optical absorption studies on PEO/PVP-based polymer blend electrolytes were carried out to determine the optical band gap (E_g) of the samples. The absorption coefficient α was determined from the spectra using the formula:

$$\alpha = 2.303 \times A/d \tag{1}$$

where A is the absorbance and d is the thickness of the film.

When a direct band gap exists, the absorption coefficient has the following dependence on the energy of the incident photon [29].

$$\alpha h\gamma = C_1\left[h\gamma - E_{gd}\right]^{1/2} \tag{2}$$

where E_{gd} is the direct band gap, C_1 is a constant dependent on specimen structure, γ is the frequency of incident light, and h is the Planck's constant. The direct and indirect band gap values of the pure PEO/PVP blend are 4.87 and 4.63 eV, respectively [10].

The direct band gaps were evaluated from $(\alpha h\gamma)^2$ vs. $h\gamma$ plots (Fig. 7), and the allowed transition energy was determined by extrapolating the linear portions of the curves to zero absorption. For sample A1, the direct band gap lies at 4.35 eV, while for the samples A2, A3, and A4, they lie at 4.45, 4.49, and 4.57 eV, respectively.

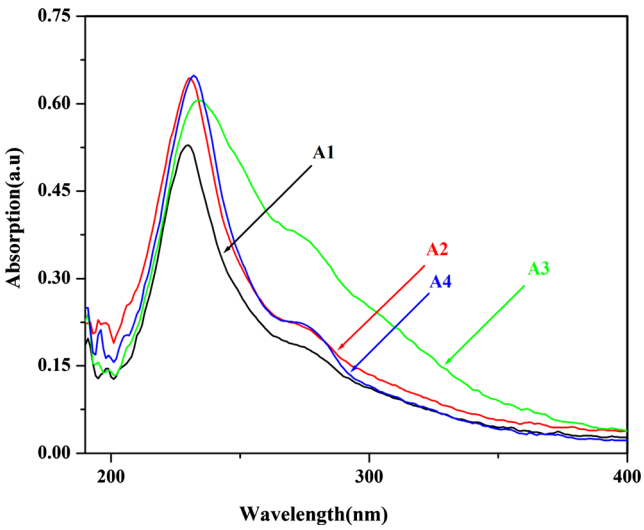

Fig. 6 Optical absorption for the prepared samples

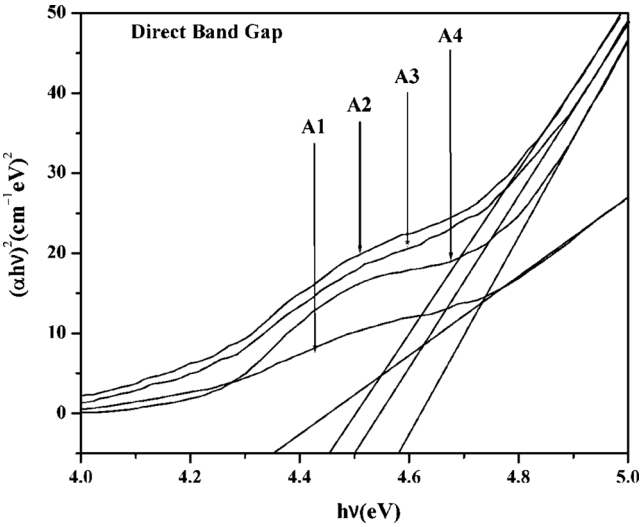

Fig. 7 Plots for the direct band gap in polymer electrolyte samples A1, A2, A3, and A4

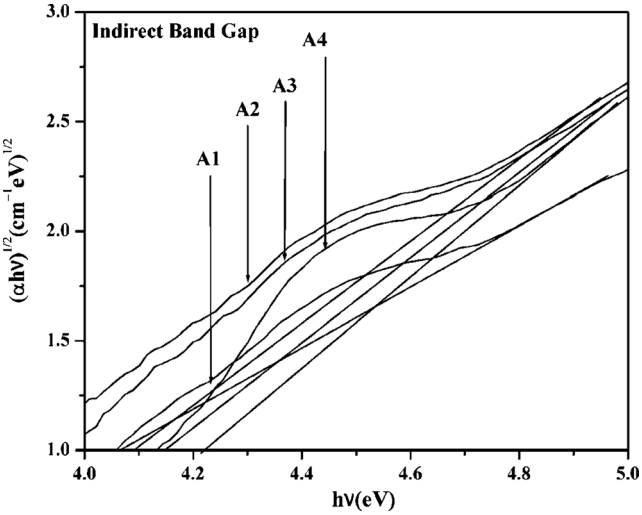

Fig. 8 Plots for indirect band gap in polymer electrolyte samples A1, A2, A3, and A4

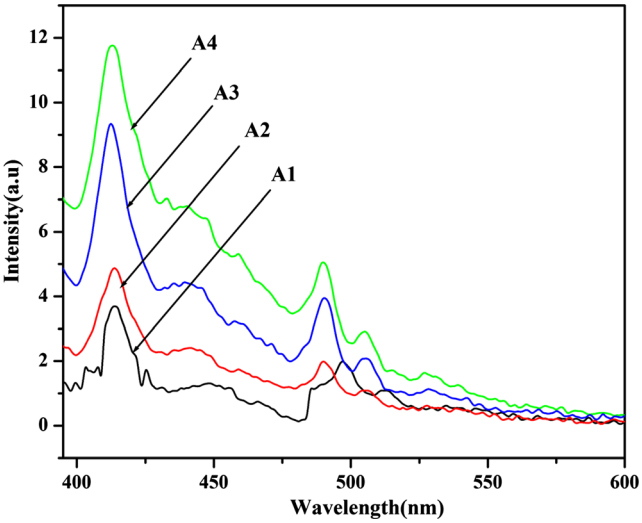

Fig. 9 Photoluminescence emission spectra of the prepared electrolyte samples

For indirect transition that requires phonon assistance, the absorption coefficient depends on the indirect photon energy according to the equation:

$$\alpha h\gamma = C_2\left[h\gamma - E_{gi}\right]^2 \tag{3}$$

where E_{gi} is the indirect band gap, C_2 is a constant dependent on specimen structure, γ is the frequency of incident light, and h is the Planck's constant. Hence, the indirect band gap values were obtained from the plots of $(\alpha h\gamma)^{1/2}$ vs. $h\gamma$ at the intercepts of the energy axis on extrapolating the linear portion of the curves to zero absorption value (Fig. 8). For the sample A1, the indirect band gap lies 4.04 eV, whereas for the samples A2, A3, and A4, they lie at 4.09, 4.15, and 4.21 eV, respectively.

The values of the direct and indirect band gap energy were shown in Table 4. From the table, we can understand that the direct and indirect band gap values decrease with the decrease of PEO content. As the band gap energy increases, the conductivity gets decreased. In other words, the decrease in the optical band gap results in an increase in the degree of disorder in the films. These results are in agreement with those obtained from XRD and conductivity studies.

Table 4 Direct and indirect optical band gap values of the prepared samples

Sample code	Ionic conductivity (σ)×10^{-5} S cm^{-1} (at 303 K)	Band gap energy (eV)	
		Direct (E_{gd})	Indirect (E_{gi})
A1	0.2307	4.35	4.07
A2	0.1778	4.45	4.09
A3	0.0628	4.49	4.15
A4	0.0404	4.57	4.21

4.6 Photoluminescence Studies

The ionic conductivity of the electrolyte is completely controlled by the local viscosity of the electrolyte sample because the ionic conductivity is directly modlinked with the viscosity. Fluorescence emission intensity is inversely proportional to the local free volume of the electrolyte medium and directly associated with the local viscosity of the medium [30].

In the present work, photoluminescence emission spectra of the prepared electrolytes are shown in Fig. 9 at an excitation wavelength of 370 nm. It is found from Fig. 9 that the sample A1 shows the minimum intensity compared to other samples which may be attributed to the minimum local viscosity of the sample. This result is also well correlated with the ionic conductivity values of the present system.

5 Conclusions

PEO- and PVP-based solid polymer blend electrolytes were successfully prepared by solvent casting technique. The high ionic conductivity was found to be 0.2307×10^{-5} S cm^{-1} for the sample A1. The temperature-dependent ionic conductivity of the present system obeys the VTF relation. The complex formation and amorphous nature of the polymer films were confirmed by FTIR and XRD analysis, respectively. The thermal stability 324 °C was obtained for the sample A1. Optical band gap (both direct and indirect) showed a decreasing trend with the increase of ionic conductivity of the blend electrolytes. The emission peaks observed from the photoluminescence were in line with the conductivity results. Hence, these data suggest that the present electrolyte system is a worthy candidate for battery applications.

Acknowledgement One of the authors, K. Kesavan, is thankful to the Department of Science and Technology (DST), New Delhi, India for the financial support provided under the DST-PURSE program.

References

1. N.S. Choi, Y.G. Lee, J.K. Park, J.M. Ko, Electrochim. Acta **46**, 1581 (2001)
2. A.M. Stephen, R. Trirunakaran, N.G. Renganathan, V. Sundaram, S. Pituchumani, N. Muniyandi, R. Gangadharan, P. Ramamoorthy, J. Power Sources **81**, 752 (1999)
3. D.E. Fenton, J.M. Parker, P.V. Wright, Polymer **14**, 589 (1973)
4. M.B. Armand, J.M. Chabagno, M. Duclot. Second international meeting on solid electrolytes, extended abstract, 1978
5. F. Croce, G.B. Appetechi, L. Persi, B. Scrosati, Nature **394**, 456 (1998)
6. F. Croce, R. Curini, A. Martinelli, L. Persi, F. Rosni, B. Scrosati, J. Phys. Chem. B **103**, 10632 (1999)
7. P.G. Bruce, *Solid state electrochemistry* (Cambridge University Press, Cambridge, 1995), p. 344
8. Y.G. Andreev, P.G. Bruce, Electrochim. Acta **45**, 1417 (2000)
9. D.A.J. Rand, J. Power Sources **4**, 01 (1979)
10. K. KiranKumar, M. Ravi, Y. Pavani, S. Bhavani, A.K. Sharma, V.V.R. NarasimhaRao, Phys. B **406**, 1706 (2011)
11. K. Kesavan, S. Rajendran, C.M. Mathew, Polym. Sci., Ser. B **56**, 520 (2014)
12. K. Xu, Chem. Rev. **104**, 4314 (2004)
13. M. Ulaganathan, S. Rajendran, J. Appl. Electrochem. **41**, 83 (2011)
14. T. Nagatomo, C. Ichikawa, O. Omoto, J. Electrochem. Soc. **134**, 305 (1987)
15. T. Nagamoto, H. Kakehata, C. Ichikawa, O. Omoto, Jpn. J. Appl. Phys. **24**, L305 (1985)
16. B.L. Papke, M.A. Ratner, D.F. Shriver, J. Electrochem. Soc. **129**, 1434 (1982)
17. G.P. Simon, Z. Shen, Y.B. Cheng., Eur. Polym. J. 39,1917 (2003)
18. Sireerat Intarakamhang. Preparation, characterization and molecular modelling of poly(ethylene oxide)/poly(vinyl pyrrolidone) montmorillonite nano-composite solid electrolytes. ISBN 974-533-520-7, pp. 54–175 (2005)
19. C.V. Subba Reddy, A.-P. Ji, Q.-Y. Zhu, L.-Q. Mai, W. Chen, Eur. Phys. J. E **19**, 471 (2006)
20. C.V.S. Reddy, X. Han, Q, Y. Zhu, L.Q. Mai, W. Chen, Microelectron. Eng. 83,281 (2006)
21. A.M. Stephan, R. Thirunakaran, N.G. Renganathan, V. Sundaram, S. Pitchumani, N. Muniyandi, S. Ramamoorthy, J. Power Sources **81**, 752 (1999)
22. M. Watanabe, K. Sanui, N. Ogata, T. Kobayashi, Z. Ohbaki, J. Appl. Phys. **57**, 123 (1985)
23. R. Bajpai, R. Palival, S.C. Datt, J. Polym. Mater. **13**, 991 (1996)
24. S. Rajendran, V. Shanthi Bama, M. Ramesh Prabhu, Ionics **16**, 283 (2010)
25. R.G. Linford, *Electrochemical science and technology of polymer. Chapter 3* (Elsevier, Appl. Science, London, 1987)
26. J.Y. Kim, S.H. Kim, Solid State Ionics 124,91 (1999
27. E.M. Abdelrazk, Phys. B **403**, 2137 (2008)
28. N.R. Rao, *Ultraviolet and visible spectroscopy: chemical applications* (Butterworth, London, 1967)
29. G.M. Thutupalli, G. Tomlin, J. Phys. D: Appl. Phys. **9**, 1639 (1976)
30. U.S. Park, Y.J. Hong, S.M. Oh, Electrochim. Acta **849** (1996)